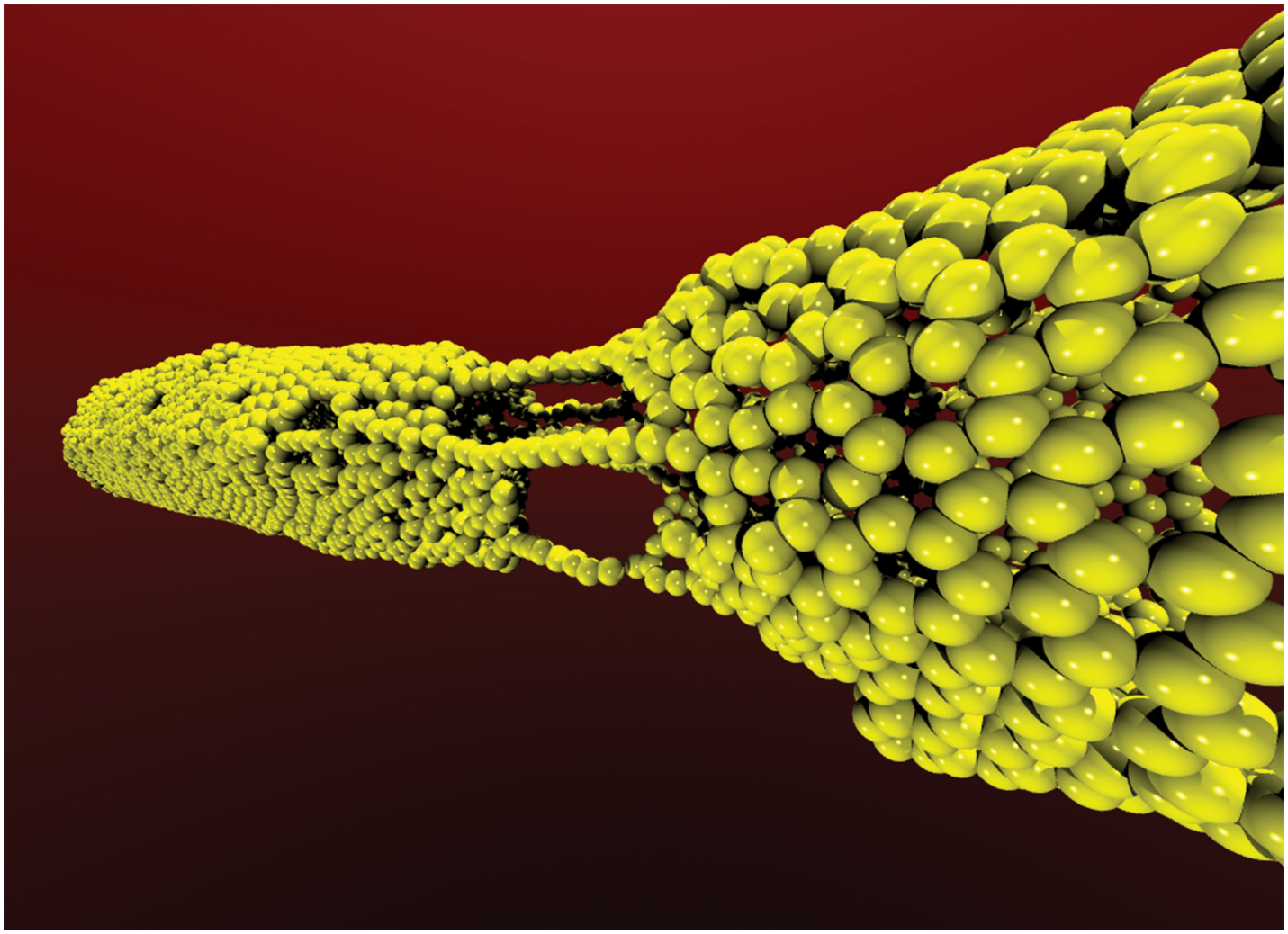

Showcasing research from the Institute of Physics at the University of Brasília, Brazil.

A reactive molecular dynamics study on the mechanical properties of a recently synthesized amorphous carbon monolayer converted into a nanotube/nanoscroll

Upon uniaxial stress, amorphous carbon nanotubes and nanoscrolls present a non-elastic regime before their total rupture. Their mechanical behavior is substantially different, thus indicating that topology plays an important role in defining their elastic properties.

As featured in:

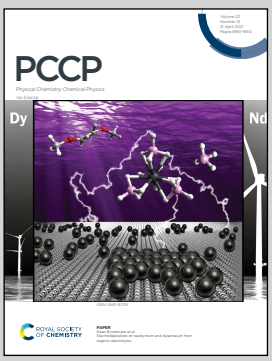

See Marcelo Lopes Pereira Junior *et al.*, *Phys. Chem. Chem. Phys.*, 2021, **23**, 9089.

ROYAL SOCIETY OF CHEMISTRY

rsc.li/pccp

Registered charity number: 207890

PCCP

ROYAL SOCIETY OF CHEMISTRY

PAPER

Published on 01 February 2021
Licence and permissions

Check for updates

Cite this: *Phys. Chem. Chem. Phys.*, 2021, **23**, 9089

A reactive molecular dynamics study on the mechanical properties of a recently synthesized amorphous carbon monolayer converted into a nanotube/nanoscroll

Marcelo Lopes Pereira Junior, *[a] Wiliam Ferreira da Cunha,[a] Douglas Soares Galvão[bc] and Luiz Antonio Ribeiro Junior [a]

Received 23rd December 2020,
Accepted 1st February 2021

DOI: 10.1039/d0cp06613c

rsc.li/pccp

Recently, laser-assisted chemical vapor deposition has been used to synthesize a free-standing, continuous, and stable monolayer amorphous carbon (MAC). MAC is a pure carbon structure composed of randomly distributed five, six, seven, and eight atom rings, which is different from that of disordered graphene. More recently, amorphous MAC-based nanotubes (a-CNT) and nanoscrolls (a-CNS) were proposed. In this work, we have investigated (through fully atomistic reactive molecular dynamics simulations) the mechanical properties and sublimation points of pristine and a-CNT and a-CNS. The results showed that a-CNT and a-CNS have distinct elastic properties and fracture patterns compared to those of their pristine analogs. Both a-CNT and a-CNS presented a non-elastic regime before their total rupture, whereas the CNT and CNS underwent a direct conversion to fractured forms after a critical strain threshold. The critical strain values for the fracture of the a-CNT and a-CNS are about 30% and 25%, respectively, and they are lower than those of the corresponding CNT and CNS cases. Although less resilient to tension, the amorphous tubular structures have similar thermal stability in relation to the pristine cases with sublimation points of 5500 K, 6300 K, 5100 K, and 5900 K for a-CNT, CNT, a-CNS, and CNS, respectively. An interesting result is that the nanostructure behavior is substantially different depending on whether it is a nanotube or a nanoscroll, thus indicating that the topology plays an important role in defining its elastic properties.

1 Introduction

Carbon-based nanomaterials have been used in numerous energy storage and conversion applications as good cost-benefit alternatives to conventional (silicon-based) technology.[1,2] Many of their promises in revolutionizing these fields still need further refining for commercial-grade applications. Among such applications are worth mentioning organic photovoltaics,[3] light-emitting diodes,[4] and thin-film transistors.[5] The broad range of carbon-based nanomaterials employed in developing these applications includes graphene and its allotropes,[6] carbon nanotubes,[7] nanoscrolls,[8] nanofibers,[9] and amorphous carbon materials.[10] Particularly, carbon nanotubes (CNTs) are still a subject of interest due to their remarkable electronic and structural properties, which have impacted several areas of nanotechnology.[11] CNTs present distinct electronic properties, such as metallic and semiconducting behavior, depending on their symmetry.[12] Carbon nanoscrolls (CNSs), in turn, are formed by the jelly or papyrus roll-like wrapping of a graphite sheet to form a tubular structure.[13–15] Recent synthesis efforts provided simple low-temperature routes to obtain CNSs.[8,16]

Amorphous carbons are families of carbon-based materials without a long-range crystalline order.[10] Several experimental efforts have been devoted to understanding the electronic and structural properties of amorphous CNTs (a-CNTs) for their applications in nanoelectronics.[17–23] The synthesis and characterization of these materials were studied through simple fabrication procedures used for preparing highly ordered nanotube arrays.[21] Electrical transport measurements on individual a-CNTs showed that their resistivity is of the same order as multiwalled CNTs despite their disordered microstructure.[22] a-CNTs were also employed as potential candidates for water purification.[23] It was reported that they can be used for adsorption and/or removal of hydroxyl group substituted aromatic compounds like Resorcinol as well as heavy metal ions like arsenic from water.

[a] *Institute of Physics, University of Brasília, Brasília 70919-970, Brazil. E-mail: marcelolpjunior@gmail.com*
[b] *Applied Physics Department, University of Campinas, Campinas, São Paulo, Brazil*
[c] *Center for Computing in Engineering and Sciences, University of Campinas, Campinas, São Paulo, Brazil*

From the theoretical point of view, the electronic properties of a-CNTs were studied by using a tight-binding model Hamiltonian.[24] Through this approach, it was determined that strong electron-lattice coupling of states near the Fermi energy leads to the formation of a bandgap.[24] This model has also predicted that the bandgap in a-CNTs has a stronger diameter dependency (inversely proportional) than CNTs. In relation to CNS, some theoretical and experimental studies were performed to address the possible synthetic routes.[8,14,16,25–29] Density functional theory (DFT) simulations were employed to investigate the atom-scale nucleation of graphene growth on the copper surface.[30–32] The formation of distributed five, six, seven, and eight carbon atom rings was achieved by modeling the chemical vapor deposition (CVD) growth of graphene. In the deposition processes, the carbon atom sinks into the copper surface. As more carbon atoms are adsorbed nearby, it will spontaneously form a dimer with one of the new adsorbed carbon atoms, and the formed dimer will up-float on top of the surface, subsequently.[31] As a consequence, random graphene islands (2D amorphous carbon material) can be formed stepwise with energetic preference. There are only a very few studies in the literature on amorphous CNS (a-CNS).[33,34] To the best of our knowledge, up to now, there have been no studies on the thermomechanical properties of a-CNTs and a-CNSs.

Very recently, laser-assisted chemical vapor deposition has been used to synthesize a free-standing, continuous, and stable monolayer amorphous carbon (MAC).[35] MAC is a pure carbon structure composed of randomly distributed five, six, seven, and eight atom rings (see Fig. 1(a)). Its lattice arrangement is different from that of disordered graphene. These findings have revealed that MAC has a high yield strength value with no crack propagation. Since the synthesis of MAC was achieved, its conversion to nanotubes and nanoscrolls emerges as a possibility.

Motivated by the recent MAC synthesis[35] and by the proposition about the existence of tubes and scrolls formed from MAC membranes,[36] in this study, the mechanical and thermal stabilities of MAC-based a-CNT and a-CNS were investigated in the framework of fully-atomistic reactive molecular dynamics simulations. The elastic properties of these model tubular materials were studied using the stress–strain relationship, and their thermal stability was analyzed by employing a heating ramp protocol. The results obtained here for these amorphous structures were contrasted against their related pristine ones.

2 Details of modeling

We have performed fully-atomistic molecular dynamics (MD) simulations using the adaptive-interatomic reactive bond-order (AIREBO)[37] potential as implemented in LAMMPS.[38] It is worthwhile to mention that *ab initio* MD simulations are commonly used to investigate the chemical reactions in nanostructures.[39,40] However, with reactive MD simulations, one can model large-scale systems where chemical reactions are occurring. Moreover, one can simulate hundreds of thousands of atoms with a substantially lower computational cost. The main focus of the present work lies in providing a comparative study of the mechanical properties of pristine and MAC-based amorphous CNTs and CNSs. All these structures were generated using the Sculptor software suite.[41] The a-CNT was obtained by binding the two lateral edges of the MAC sheet,[35,42] whereas the a-CNS was formed by a spiral-like roll-up of the MAC sheet with open edges at both ends, with a rolling angle of 4π. Fig. 1 shows the representation of the MAC sheet (Fig. 1(a)),

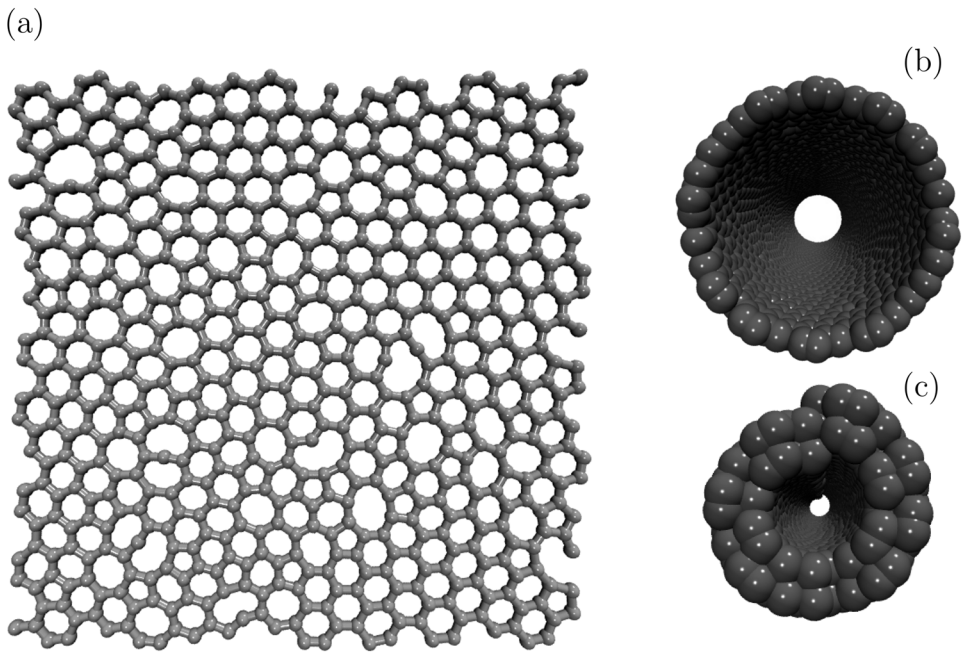

Fig. 1 Structural models of the (a) MAC sheet and its related (b) a-CNT and (c) a-CNS atomistic structures.

its derived nanotube (Fig. 1(b)), and nanoscroll (Fig. 1(c)). The MAC atomistic structure used here to build our model a-CNT contains 610 atoms.[35,42] The obtained a-CNT has a diameter of 25 Å and a length of 120 Å, and it was formed by merging six MAC sheets (2 in the *x*-direction and 3 in the *y*-direction), totaling 3660 atoms. In this study, a MAC sheet was considered as a unit cell. The a-CNS has also a length of 120 Å, but it has an internal and external diameter of 10 Å and 16 Å, respectively. The quantity of MAC sheets and the total number of atoms used to build the a-CNS are equal to those in the a-CNT case.

Our computational approach is based on submitting the systems to tensile deformation to address their elastic properties as well as to a heating ramp process to obtain their estimated sublimation points. These analyses were performed by considering the virial stress tensor.[43] We also calculated the von Mises stress[44] as it is an important tool to describe the stretching dynamics and fracture patterns of the systems.[45]

As for the heating ramp procedure, it consisted of a linear temperature increase in a *NVT* ensemble in which a temperature range of from 0 up to 10 000 K was performed after a preliminary thermalization procedure within an *NPT* ensemble. The temperature ramp rate was set to approximately 200 K ms^{-1}. The temperature and pressure were controlled through an *NPT* ensemble by employing the Nosé–Hoover thermostat.[46] The MD snapshots and trajectories were obtained by using free visualization and analysis software VMD.[41] The equations of motion were numerically integrated using a velocity-Verlet integrator with a time-step of 0.1 fs. Importantly, it was demonstrated that time steps above 0.5 fs are not reliable for predicting the mechanical responses of carbon-based nanostructures in the context of reactive MD force fields.[47] The total time of simulations was 6 ns, which is enough time to realize the fracture dynamics of all the systems studied here. Before applying the uniaxial stretching, thermalization within an *NVT* ensemble was performed at 300 K for 500 ps (5 000 000 MD-steps) to eliminate any residual stresses. We increased the tensile stress in the system by applying a uniaxial strain along the longitudinal direction of the tubular structures, with an engineering strain rate of 1.0 × 10^{-7} fs^{-1}.

3 Results

Initially, we investigated the stress–strain behavior of both systems: the a-CNT (Fig. 2(a)) and a-CNS (Fig. 2(b)). In both figures, we present the results of the structures derived from the pristine nanosheet in blue and of the amorphous one in red. In both the scenarios, the curves more or less overlap until a critical strain value is achieved. Such a critical strain value indicates the phase transition in the stress–strain dependence, which consists of the point of fracture of each structure. The fracture strain, for each case, is as follows: 27%, 48%, 24%, and 34% for a-CNT, CNT, a-CNS, and CNS, respectively.

As expected, the general trend is that the pristine (defectless) structures can stand larger strain values without fracturing. Fig. 2(a) shows that CNT is able to stand roughly 20% more strain than its amorphous counterpart. Fig. 2(b) compares the amorphous and pristine versions of the nanoscroll. This figure shows that the pristine nanoscroll upholds 15% more strain than its amorphous version. This trend is consistent with the fact that highly ordered carbon systems, such as graphene, will be tougher than their defective structures.[48] Such strength arises from the strong overlap of the sp2 hybrid orbitals. When the sites are uniformly close to each other, as is the case of the pristine scenario, the collective effect is that all the regions of the nanostructure exhibit the same strength. In the amorphous case, as two carbon cores approach one another, the relative strength between these two becomes stronger. However, as a consequence, the distance to the third core becomes larger and, therefore, the interaction is weaker. As the structure as a whole is only as strong as its weakest

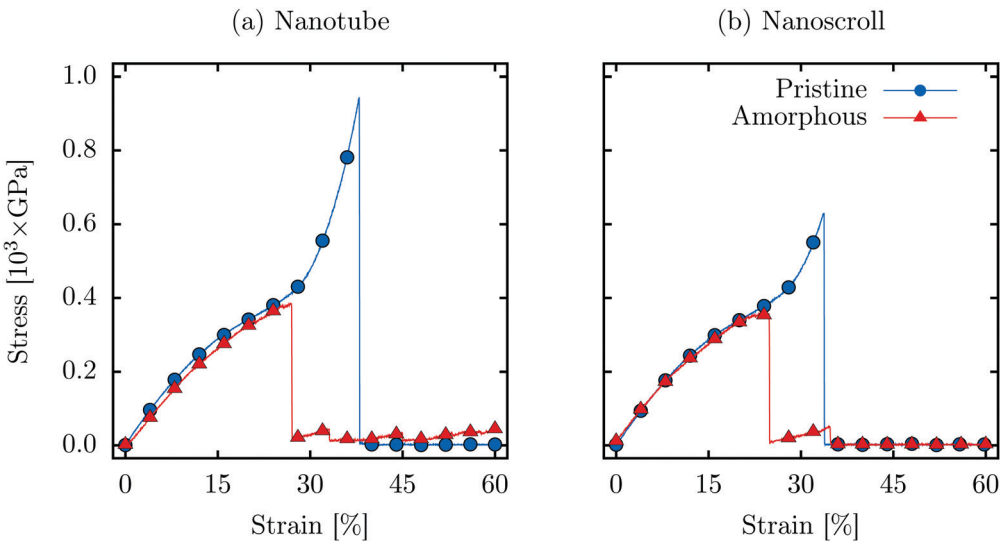

Fig. 2 Stress–strain curves for (a) CNT (blue) and a-CNT (red) and (b) for CNS (blue) and a-CNS (red) at 300 K, considering the uniaxial strain applied in the longitudinal direction. The structures were stretched at a constant elongation rate until total rupture.

bond, it is expected that the amorphous tends to be weaker than the pristine systems.

Another crucial feature of this set of simulations is observed through the comparison between Fig. 2(a) and (b). We can observe that the nanostructure behavior is substantially different depending on whether it is a nanotube or a nanoscroll, thus indicating that the topology plays a crucial role in defining its elastic properties (see also Table 1).

Table 1 summarizes the set of elastic properties obtained from MD simulations for the systems illustrated in Fig. 1. It is worthwhile to stress that previous works have described the low-strain region as being quadratic due to the strong non-linear behavior in the elastic regime.[49–51] In this way, the stress–strain relationship is given by $\sigma = E\varepsilon + D\varepsilon^2$, where σ, ε, E, and D are the symmetric second Piola–Kirchhoff stress, uniaxial strain, Young's modulus, and third-order elastic modulus, respectively.[52] Note that LAMMPS calculates Second Piola–Kirchhoff stress by default, using the Lagrangian description of the system.[38] In the table, E stands for Young's modulus, D is the third-order elastic modulus, TS is the tensile strength and ε_F is the critical strain for the fracture. These values are numerical representations of the response of each material to the processes reported in Fig. 2. As expected, the pristine structures presented a higher Young's modulus when contrasted with their amorphous analogs. However, these values are reasonably close. The more cohesive nature of CNTs endows this material with higher tensile strength and critical strain for the fracture. Due to the very nature of the system structures, the applied tensions are uniaxial and, therefore, the Young's modulus is a measure of the system stiffness.

In Fig. 3 and 4 we present the representative MD snapshots of the fracturing processes of the different systems considered here and the von Mises stress distribution along the nanostructure. In these figures, the (a) and (b) sequence of panels illustrate the representative MD snapshots for the pristine and amorphous cases, respectively. Note that the a-CNT and a-CNS have a smaller fracture point in terms of strain in an approximate 1:4 ratio, which is consistent with the results presented in Fig. 2. The trend of the amorphous structure to present smaller cutoff stress is preserved and rather similar among these two types of amorphous structures. Another clear trend to be observed is the appearance of linear atomic chains (LACs) before rupture, in both types of amorphous nanostructures. The same is not observed for pristine nanotubes and nanoscrolls. Due to the absence of porosity, CNTs and CNS go from integrity to their fractured form abruptly. From these facts, one

Table 1 Elastic properties of MAC and graphene nanotubes and nanoscrolls. E, D, TS, and εF refer to the Young's Modulus, third-order elastic modulus, TS tensile strength, and critical strain, respectively

System	E [GPa]	D [GPa]	TS [GPa]	ε_F [%]
MAC nanotube	2268.67	3001.13	384.97	26.72
Graphene nanotube	2495.51	3927.15	944.36	37.96
MAC nanoscroll	2476.61	3843.84	359.59	23.56
Graphene nanoscroll	2493.82	4460.73	630.82	33.76

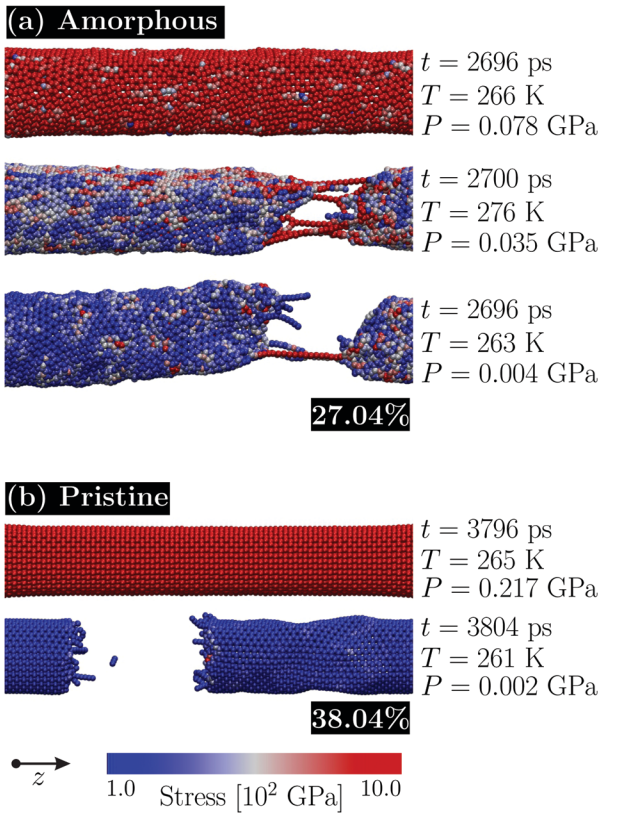

Fig. 3 Representative MD snapshots for the fracture process of (a) a-CNT and (b) pristine CNT.

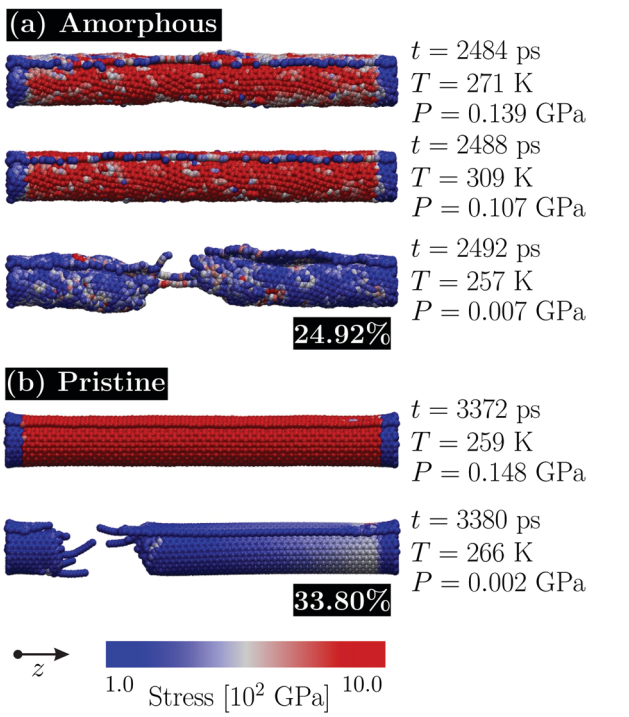

Fig. 4 Representative MD snapshots for the fracture process of (a) a-CNS and (b) pristine CNS.

can again conclude that the structural disorder is of greater importance than the topological aspects.

In Fig. 5 we present the interplay between the total energy of the system and the thermal bath to it. The thermalization process for nanotubes (Fig. 5(a)) and nanoscrolls (Fig. 5(b)) is rather similar. For low temperatures, the curves are almost parallel, and the energy absorption of the amorphous cases is slightly smaller than that of the pristine ones. A feature that can be readily observed is that, as temperature increases, the relationship between these two quantities behavior for amorphous (red triangles) and pristine (blue circles) nanostructures is less important. This trend should, indeed, be expected, because higher temperature introduces disorder effects to the pristine chain, thus increasing the random degree of the atom movements, as is the case of the amorphous structure. A comparison between the two figures shows that the nanotubes absorb the thermal energy more efficiently than the nanoscrolls. This difference can be explained by the fact the scrolls have an open structure that allows converting the thermal energy into kinetic energy.

Fig. 5 also allows us to have insights into the sublimation point of the nanostructures. As a general trend, the total energy increases linearly with the temperature and shows two well-defined regimes with different slopes. The discontinuity in these curves is suggestive of a phase transition from a solid to a gas-like phase. A gas-like phase denotes a system configuration in which the carbon atoms are isolated or bonded in small LACs (with 5 atoms at most), yielding a smaller concentration of atoms when contrasted with the CNT and CNS cases before sublimation (see Fig. 6). The transition between these two behaviors defines the sublimation point. This abrupt change in the slope of the curves is related to a gain in kinetic energy due to the higher atom velocities in the gas-like phase, which increases the total energy. Moreover, part of the harmonic and torsional energies in the solid phase were also converted into kinetic energy, which again contributes to the increase in the total energy of the system in the gas-like phase. The amorphous tubular structures have similar thermal stability when contrasted to the pristine cases with sublimation points of 5500 K, 6300 K, 5100 K, and 5900 K for a-CNT, CNT, a-CNS, and CNS, respectively.

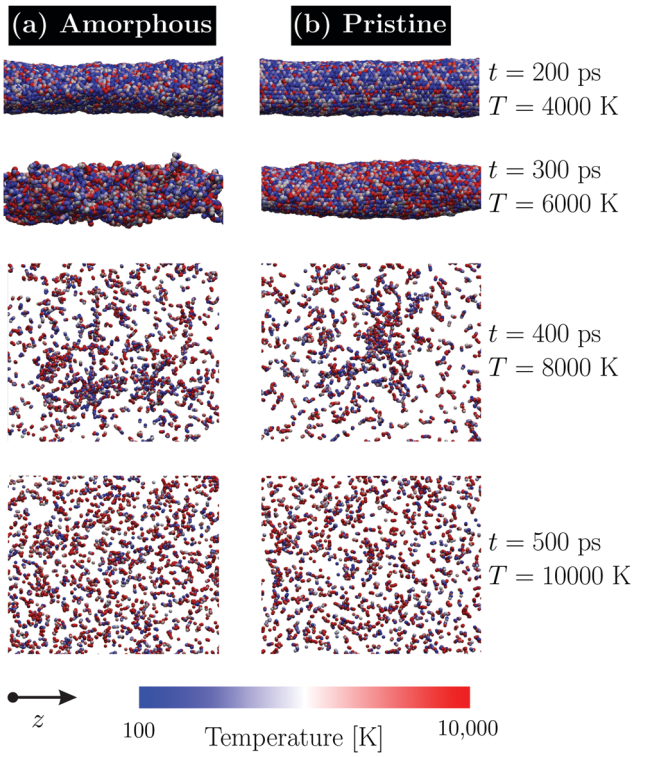

Fig. 6 Representative MD snapshots of the heating simulations for (a) a-CNT and (b) pristine CNT. At 10 000 K only the gas-like phase takes place.

In Fig. 6 and 7 we show the representative MD snapshots for the heating simulations for the nanotubes and nanoscrolls, respectively. In these figures, the (a) and the (b) sequence of panels depict the MD snapshots for the amorphous and pristine cases, respectively. In Fig. 6, we can see that the a-CNT starts to lose its integrity, whereas the pristine is still stable at 6000 K.

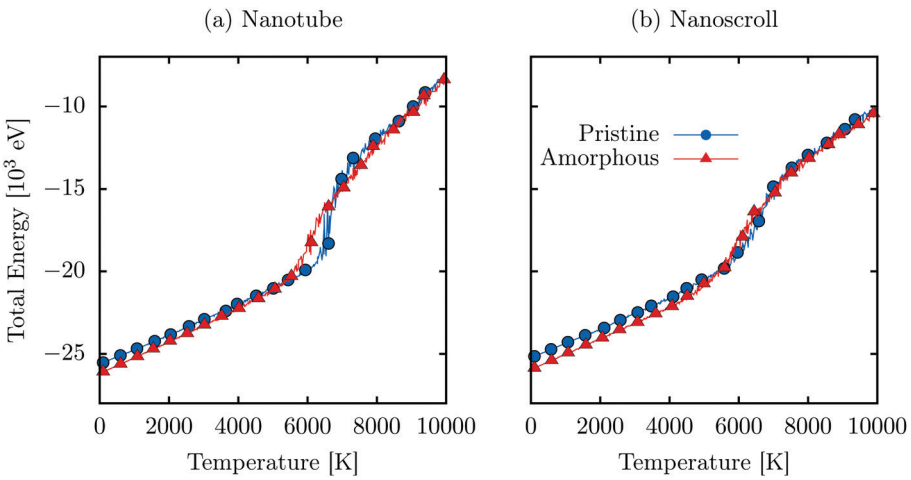

Fig. 5 Total energy as a function of temperature for (a) nanotubes and (b) nanoscrolls. Amorphous structures are represented by red triangles and pristine ones by blue circles.

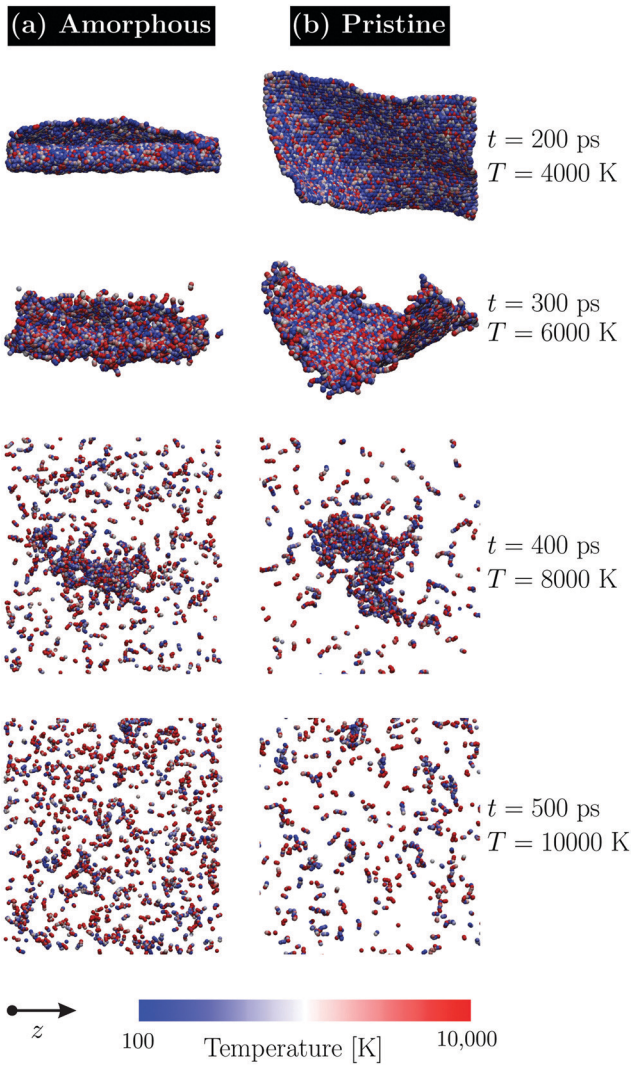

Fig. 7 Representative MD snapshots of the heating simulations for (a) a-CNS and (b) pristine CNS. At 10 000 K only the gas-like phase takes place.

At 8000 K, both structures have reached their sublimation point, and a partially gas-like phase is observed. In the case of nanoscrolls (Fig. 7), the pristine structure loses its structural integrity at 4000 K, whereas the amorphous one at 5100 K. As in the case of CNTs, at 8000 K just a partially gas-like phase is observed, although more pronounced. From this set of simulations, it can be concluded that nanotubes are more thermally stable than nanoscrolls. As a general trend, one can also conclude that pristine structures are more stable than their amorphous counterparts, for the same reasons as the mechanical behavior discussed above.

4 Conclusions

In summary, we have investigated (through fully atomistic reactive molecular dynamics simulations) the mechanical properties and sublimation points of pristine and amorphous carbon nanotubes and carbon nanoscrolls. The amorphous structures are based on the recently synthesized[35] stable monolayer amorphous carbon (MAC). Our results show that amorphous carbon nanotubes present lower tensile-strength than their corresponding pristine ones, which is expected since in general defectless structures are tougher than defective ones. The pristine structures exhibit abrupt fracture dynamics while the amorphous ones present intermediate states before complete failure. However, all structures exhibit a linear atomic carbon chain structure before their rupture. The stress–strain curves for pristine/amorphous structures more or less overlap until the critical strain value is reached. The fracture strain, for each case, is as follows: 27%, 48%, 24%, and 34% for a-CNT, CNT, a-CNS, and CNS, respectively. An interesting result is that the nanostructure behavior is substantially different depending on whether it is a nanotube or a nanoscroll, thus indicating that the topology plays an important role in defining its elastic properties. The nanotubes of both symmetries present higher sublimation points than nanoscrolls, suggesting that the tubes are thermally more stable than the scrolls. In the case of amorphous nanotubes, a thermal critical value of 6000 K was obtained, at which point the pristine nanoscroll, for instance, had already lost its structural integrity. It is well accepted that carbon nanotubes and nanoscrolls are considerably stiffer than graphene sheets. The experimental Young's modulus for graphene is about 1000 GPa.[53] In the present work, the Young's modulus for pristine and amorphous carbon nanotubes and nanoscrolls ranged from 2200 up to 2500 GPa. Such differences in the Young's modulus of tubular (1D) structures, when contrasted with that of the monolayer (2D) ones, can be understood by their different topologies, which affect their elasticity/flexibility.

Conflicts of interest

There are no conflicts to declare.

Acknowledgements

The authors gratefully acknowledge the financial support from Brazilian research agencies CAPES, CNPq, FAPESP, and FAP-DF. M. L. P. J. gratefully acknowledges the financial support from CAPES grant 88882.383674/2019-01. D. S. G. acknowledges the Center for Computing in Engineering and Sciences at Unicamp for financial support through the FAPESP/CEPID Grants #2013/08293-7 and #2018/11352-7. L.A.R.J. gratefully acknowledges the financial support from CNPq grant 302236/2018-0 and the financial support from FAP-DF grant 0193.0000248/2019 – 32. L. A. R. J. gratefully acknowledges the financial support from DPI/DIRPE/UnB (Edital DPI/DPG 03/2020) grant 23106.057541/2020 – 89 and from IFD/UnB (Edital 01/2020) grant 23106.090790/2020 – 86.

Notes and references

1 B. Bayatsarmadi, Y. Zheng, A. Vasileff and S.-Z. Qiao, *Small*, 2017, **13**, 1700191.

2 M. S. Mauter and M. Elimelech, *Environ. Sci. Technol.*, 2008, **42**, 5843–5859.
3 B. Kippelen and J.-L. Brédas, *Energy Environ. Sci.*, 2009, **2**, 251–261.
4 B. Geffroy, P. Le Roy and C. Prat, *Polym. Int.*, 2006, **55**, 572–582.
5 H. Klauk, *Chem. Soc. Rev.*, 2010, **39**, 2643–2666.
6 A. N. Enyashin and A. L. Ivanovskii, *Phys. Status Solidi B*, 2011, **248**, 1879–1883.
7 S. Iijima, *Nature*, 1991, **354**, 56–58.
8 L. M. Viculis, J. J. Mack and R. B. Kaner, *Science*, 2003, **299**, 1361–1362.
9 E. Hammel, X. Tang, M. Trampert, T. Schmitt, K. Mauthner, A. Eder and P. Pötschke, *Carbon*, 2004, **42**, 1153–1158.
10 J. Robertson, *Adv. Phys.*, 1986, **35**, 317–374.
11 R. C. Haddon, *Acc. Chem. Res.*, 2002, **35**, 997.
12 V. N. Popov, *Mater. Sci. Eng., R*, 2004, **43**, 61–102.
13 R. Bacon, *J. Appl. Phys.*, 1960, **31**, 283–290.
14 S. F. Braga, V. R. Coluci, S. B. Legoas, R. Giro, D. S. Galvão and R. H. Baughman, *Nano Lett.*, 2004, **4**, 881–884.
15 D. Tománek, *Phys. B*, 2002, **323**, 86–89.
16 H. Shioyama and T. Akita, *Carbon*, 2003, **41**, 179–181.
17 L. Ci, B. Wei, C. Xu, J. Liang, D. Wu, S. Xie, W. Zhou, Y. Li, Z. Liu and D. Tang, *J. Cryst. Growth*, 2001, **233**, 823–828.
18 J. M. Calderon Moreno and M. Yoshimura, *J. Am. Chem. Soc.*, 2001, **123**, 741–742.
19 L. Ci, H. Zhu, B. Wei, C. Xu and D. Wu, *Appl. Surf. Sci.*, 2003, **205**, 39–43.
20 Y. Chen, Z. Lu, L. Zhou, Y.-W. Mai and H. Huang, *Energy Environ. Sci.*, 2012, **5**, 7898–7902.
21 Y. Lei, K.-S. Yeong, J. Thong and W.-K. Chim, *Chem. Mater.*, 2004, **16**, 2757–2761.
22 T. Hayashi, T. C. O'Connor, K. Higashiyama, K. Nishi, K. Fujisawa, H. Muramatsu, Y. A. Kim, B. G. Sumpter, V. Meunier and M. Terrones, *et al.*, *Nanoscale*, 2013, **5**, 10212–10218.
23 P. Bhowmick, D. Banerjee, S. Santra, D. Sen, B. Das and K. Chattopadhyay, *RSC Adv.*, 2016, **6**, 8913–8922.
24 A. Rakitin, C. Papadopoulos and J. Xu, *Phys. Rev. B: Condens. Matter Mater. Phys.*, 2000, **61**, 5793–5796.
25 E. Perim, L. D. Machado and D. S. Galvao, *Front. Mater.*, 2014, **1**, 31.
26 X. Xie, L. Ju, X. Feng, Y. Sun, R. Zhou, K. Liu, S. Fan, Q. Li and K. Jiang, *Nano Lett.*, 2009, **9**, 2565–2570.
27 E. Perim, R. Paupitz and D. S. Galvao, *J. Appl. Phys.*, 2013, **113**, 054306.
28 V. Dravid, X. Lin, Y. Wang, X. Wang, A. Yee, J. Ketterson and R. P. Chang, *Science*, 1993, **259**, 1601–1604.
29 H. Shioyama and T. Akita, *Carbon*, 2003, **41**, 179–181.
30 Y. Li, M. Li, T. Gu, F. Bai, Y. Yu, T. Mwenya and Y. Yu, *AIP Adv.*, 2013, **3**, 052130.
31 Y. Li, M. Li, T. Gu, F. Bai, Y. Yu, M. Trevor and Y. Yu, *Appl. Surf. Sci.*, 2013, **284**, 207–213.
32 Y. Li, M. Li, T. Wang, F. Bai and Y.-X. Yu, *Phys. Chem. Chem. Phys.*, 2014, **16**, 5213–5220.
33 Z. Gong, J. Shi, B. Zhang and J. Zhang, *Carbon*, 2017, **116**, 310–317.
34 P. Yadav, S. Warule, J. Jog and S. Ogale, *Solid State Commun.*, 2012, **152**, 2092–2095.
35 C.-T. Toh, H. Zhang, J. Lin, A. S. Mayorov, Y.-P. Wang, C. M. Orofeo, D. B. Ferry, H. Andersen, N. Kakenov and Z. Guo, *et al.*, *Nature*, 2020, **577**, 199–203.
36 R. M. Tromer, L. C. Felix, L. A. Ribeiro and D. S. Galvao, 2020, arXiv preprint arXiv:2007.05062.
37 S. J. Stuart, A. B. Tutein and J. A. Harrison, *J. Chem. Phys.*, 2000, **112**, 6472–6486.
38 S. Plimpton, *J. Comput. Phys.*, 1995, **117**, 1–19.
39 J. Wu, J.-H. Li and Y.-X. Yu, *Phys. Chem. Chem. Phys.*, 2020, **22**, 7633–7642.
40 J. Wu, J.-H. Li and Y.-X. Yu, *ChemPhysChem*, 2020, **21**, 2539–2549.
41 W. Humphrey, A. Dalke and K. Schulten, *et al.*, *J. Mol. Graphics*, 1996, **14**, 33–38.
42 L. C. Felix, R. M. Tromer, P. A. Autreto, L. A. Ribeiro Junior and D. S. Galvao, *J. Phys. Chem. C*, 2020, **124**, 14855–14860.
43 A. K. Subramaniyan and C. Sun, *Int. J. Solids Struct.*, 2008, **45**, 4340–4346.
44 R. V. Mises, Nachrichten von der Gesellschaft der Wissenschaften zu Göttingen, Mathematisch-Physikalische Klasse, **1913**, **1913**, 582–592.
45 M. L. P. Júnior and L. A. R. Júnior, *FlatChem*, 2020, **24**, 100196.
46 W. G. Hoover, *Phys. Rev. A: At., Mol., Opt. Phys.*, 1985, **31**, 1695.
47 B. D. Jensen, K. E. Wise and G. M. Odegard, *J. Comput. Chem.*, 2015, **36**, 1587–1596.
48 A. Shekhawat and R. O. Ritchie, *Nat. Commun.*, 2016, **7**, 1–8.
49 C. Lee, X. Wei, J. W. Kysar and J. Hone, *Science*, 2008, **321**, 385–388.
50 A. Zandiatashbar, G.-H. Lee, S. J. An, S. Lee, N. Mathew, M. Terrones, T. Hayashi, C. R. Picu, J. Hone and N. Koratkar, *Nat. Commun.*, 2014, **5**, 1–9.
51 T. Zhong, J. Li and K. Zhang, *J. Appl. Phys.*, 2019, **125**, 175110.
52 R. Thurston and K. Brugger, *Phys. Rev.*, 1964, **133**, A1604.
53 C. Lee, X. Wei, J. W. Kysar and J. Hone, *Science*, 2008, **321**, 385–388.